Review of Scientific Instruments ARTICLE scitation.org/journal/rsi

A method for improving temperature measurement accuracy on an infrared thermometer for the ambient temperature field

Cite as: Rev. Sci. Instrum. 91, 054903 (2020); doi: 10.1063/1.5121214
Submitted: 23 July 2019 • Accepted: 21 April 2020 •
Published Online: 7 May 2020

Shuanglong Cui, Bojun Sun, and Xiaogang Sun[a)]

AFFILIATIONS

School of Instrumentation Science and Engineering, Harbin Institute of Technology, Harbin 150001, China

[a)]Author to whom correspondence should be addressed: sxg@hit.edu.cn

ABSTRACT

In order to improve the accuracy of an infrared thermometer, the main uncertainty sources of the system are analyzed and a compensation function is established on the basis of these corrections. The verification experiments are carried out by using a self-developed infrared thermometer and a blackbody. The experimental results indicate that the compensation function can reduce the infrared thermometer expanded uncertainty from ±3.6 °C to ±1.9 °C in the temperature range of −40 °C to 60 °C. This method can effectively improve the temperature measurement accuracy of an ambient temperature infrared thermometer in its measurement range.

I. INTRODUCTION

Infrared temperature measurement technology has the advantages of non-contact, quick response, and no damage of the target.[1] However, the obtainable accuracy has traditionally been a hot research topic. In order to improve this accuracy, a great number of research studies have been carried out in the past. In 1979, Helfrich used a blackbody to calibrate the relationship between the signal of a gray body and its temperature and corrected the lack of uniformity of the infrared focal plane array by the two-point calibration method to the improve measurement accuracy.[2] In 1986, Zhang, Zhang, and Klemas used an equivalent blackbody method to reduce the influence of the ambient temperature.[3] In 1995, Chrzanowski studied the influence of the distance between the temperature measurement system and the target[4] and the impact of other system parameters on the temperature measurement accuracy.[5] In 2005, Zhang, Yang, and Liu developed a non-uniform high-temperature environmental interference model to reduce the impact of high-temperature sources near the measured target on the measurement accuracy.[6] In 2011, Zhang, Qi, and Fu used a combination of a broadband filter and a three-level interference filter to eliminate the interference of external radiation in a complex environment, thus improving the accuracy of the temperature measurement system.[7–9] In 2019, Sun and Pan studied the influence of Gauss noise and salt–pepper noise on the infrared temperature measurement accuracy in an indoor ambient and proposed an improved mean method to decrease the measurement error.[10]

Analyzing the main uncertainty sources of an infrared thermometer, the present paper establishes a compensation function to improve the accuracy of temperature measurement. The experiments carried out to calibrate the equipment are used to find out the parameters included in the compensation function. So, the resulting accuracy is meaningfully improved.

II. PRINCIPLE OF CALIBRATION AND TEMPERATURE MEASUREMENT

Infrared devices must be calibrated to establish the quantitative relationship between the input radiation intensity and the output of the infrared detector before their use.[11] The accuracy of the calibration directly affects the accuracy of measurement,[12] being one of the major sources of the type B uncertainty according to the GUM.[13]

The ambient temperature infrared thermometer presented in this paper is based on a cooled photovoltaic detector.[14] If the detector output is linear with its irradiance from the IR source,[14,15] the calibration function results in

$$V = k \cdot L + b, \tag{1}$$

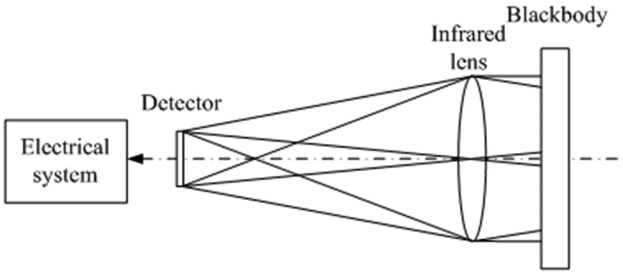

FIG. 1. Sketch of the experimental setup of infrared calibration.

where V is the detector output voltage, L is the irradiance received by the detector, k is the system response factor, and b is the system bias. The sketch of the experimental setup of infrared calibration is shown in Fig. 1.[16]

When the blackbody radiation emission completely covers the entrance pupil field of the infrared device during calibration, the total irradiation received by using the detector is the radiation exitance of the blackbody. It can be expressed through the following equation:[16,17]

$$L = \int_{\lambda_1}^{\lambda_2} R_\lambda L_{\lambda B}(T)d\lambda = \int_{\lambda_1}^{\lambda_2} R_\lambda \cdot \frac{c_1}{\pi\lambda^5} \cdot \frac{1}{e^{c_2/\lambda T} - 1} d\lambda = f(T), \quad (2)$$

where λ_2 and λ_1 are the upper and lower limits of the spectral response of the detector, T is the target absolute temperature, R_λ is the wavelength function of thermometer (the product of the spectral sensitivity of the sensor and the spectral transmittance of the optical system),[18] $L_{\lambda B}(T)$ is the blackbody radiation exitance at T temperature, and c_1 and c_2 are the first and second Plank's radiation constants.

The calibration coefficients of Eq. (1) are determined through the least squares fitting the radiation exitance vs the response at different temperatures.[19]

When calibration results are used to measure the temperature of a blackbody, focusing the thermometer on it, the target radiation exitance L is calculated from the output voltage with Eq. (1), and then, the target temperature T is calculated inverting Eq. (2). So, the following equation is obtained:

$$T = f^{-1}(L) = f^{-1}[(V - b)/k]. \quad (3)$$

If the target is a non-blackbody, but a gray body (with constant emissivity ε), this equation must be corrected,[20] and the following equation is obtained:

$$T = f^{-1}\left[\frac{\frac{V-b}{k} - (1-\varepsilon)f(T_u)}{\varepsilon}\right], \quad (4)$$

where T_u is the ambient temperature (which behaves as a blackbody, being a cavity).

III. PROPOSED METHOD TO IMPROVE MEASUREMENT ACCURACY

Calibration accuracy is one of the most important components of the type B uncertainty according to the GUM.[13] However, calibration can be further improved through a compensation method, as in the case, presented in this paper, of the homemade infrared thermometer built in the authors' laboratory.

A. Experimental device

The infrared thermometer and the blackbody used in the experiment are shown in Fig. 2. Features and technical data are as follows:

- Thermometer temperature measuring range: −40 °C to 60 °C
- Thermometer response bandwidth: 8–11 μm
- Thermometer calibration function: $V = 0.0310 * L + 1.0574$ (according to the calibration experiment thereafter described)
- Blackbody emissivity: >0.95
- Blackbody temperature resolution: 0.1 °C
- Blackbody temperature control range: −40 °C to 60 °C.

B. Calibration experiment

After manufacturing and connecting the hardware for data acquisition, the homemade infrared thermometer is calibrated comparing the blackbody radiation exitance L (calculated from the blackbody temperature) with the output signal of the instrument. Calibration data are shown in Table I.

These data are fitted using Eq. (1) as the model, leading to the following results:

$$V = 0.0310 * L + 1.0574, \quad (5)$$

with correlation coefficient 0.9995 and a standard uncertainty of voltage estimation 0.0086 V. The standard uncertainties of coefficients b and k come from the square root of diagonal elements of the covariance matrix of the unknowns and result 0.0002 and 0.004, respectively.[21] From the fitting results [Fig. 3(a)], voltage data show good linearity vs temperature.

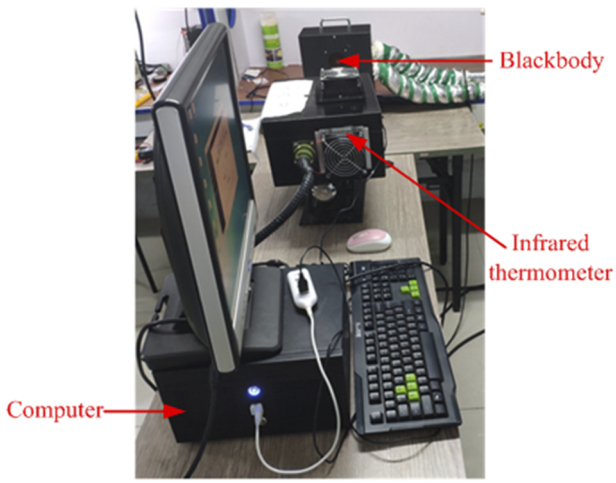

FIG. 2. Infrared thermometer and blackbody for the experiment.

TABLE I. Calibration experimental data.

Number	1	2	3	4	5
Temperature (°C)	−40.0	−35.8	−31.6	−27.6	−23.3
Voltage (V)	1.241 09	1.257 87	1.275 22	1.294 48	1.318 01
Number	6	7	8	9	10
Temperature (°C)	−14.5	−5.9	1.0	9.8	18.0
Voltage (V)	1.364 47	1.432 16	1.502 23	1.592 06	1.683 41
Number	11	12	13	14	15
Temperature (°C)	28.1	37.5	48.4	56.8	62.4
Voltage (V)	1.807 47	1.936 87	2.095 04	2.231 67	2.327 74

Exitance is converted to temperature by using Eq. (2) and then plotted in Fig. 3(b), showing the typical non-linear trend of Eq. (2). Figure 3 shows how T can be calculated from V using Eq. (4).

C. Uncertainty analysis

According to the GUM,[13] two main types of uncertainties are present: type A (evaluated with statistical methods) and type B (nonstatistical).

1. Type A uncertainty

The blackbody temperature is measured with the calibrated infrared thermometer in the temperature range −40 °C to 60 °C, and each temperature is repeated a meaningful number of times (about 15). The experimental data are recorded. Then, another target temperature is selected for a total amount of 23 different temperatures. Figure 4 reports the measurement error, i.e., the difference between the temperature set on the blackbody and the one detected by using the infrared thermometer.

Data overlap and form clouds in Fig. 4(a). Standard deviation of repeated measurements at each temperature is calculated and shown in Fig. 4(b). It is evident that the standard deviation of repeated measurements depends on temperature and varies between 0.05 °C and 0.31 °C. The maximum value of the standard uncertainty is calculated,

$$u_A = std/\mathrm{sqrt}(n) = 0.07\,^{\circ}\mathrm{C},$$

where *std* is the standard deviation and n is the number of repeated measurements.

2. Type B uncertainty

This is due to the previous knowledge of instruments and phenomena: uncertainty of set temperature values, calibration, etc.

a. Uncertainty component introduced by calibration accuracy. According to the calibration experiment, the standard uncertainty of voltage estimation is 0.0086 V. In addition, the sensitivity is calculated deriving the calibration function [Eqs. (1) and (2)] using the Wien approximation and the so-called "effective wavelength," λ_{eff},[22] in the response bandwidth of the detector. It can be expressed by the following equation:

$$\frac{dT}{dV} \approx \frac{c_2}{\lambda_{\mathrm{eff}}(V-b)\ln\left(\frac{V-b}{k\cdot\Delta\lambda\cdot R_\lambda\cdot c_1/\pi\lambda_{\mathrm{eff}}^5}\right)^2}, \tag{6}$$

where k and b come from the calibration function and $\Delta\lambda$ is the detector response bandwidth.

The sensitivity is plotted vs the voltage in the range of 1.2–2.4 V and shown in Fig. 5. It shows that the sensitivity decreases rapidly with the increase in the voltage. When the voltage is 1.24 V, the sensitivity is 196.2 and the standard uncertainty is 1.69 °C, that is, $u_{B1} = 1.69\,^{\circ}\mathrm{C}$.

b. Uncertainty component introduced by the target temperature indication value. According to the specifications of the PT100 sensors used to measure the blackbody temperature, the uncertainty component introduced by the target temperature indication value is 0.3 °C, that is, $u_{B2} = 0.3\,^{\circ}\mathrm{C}$.

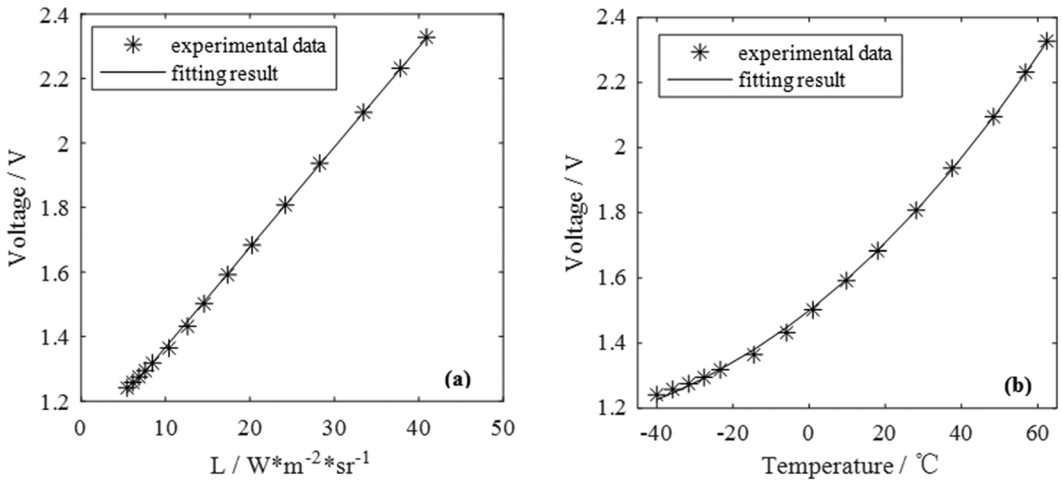

FIG. 3. Calibration effect diagram: (a) the fitting curve of V and L and (b) the fitting curve of V and T.

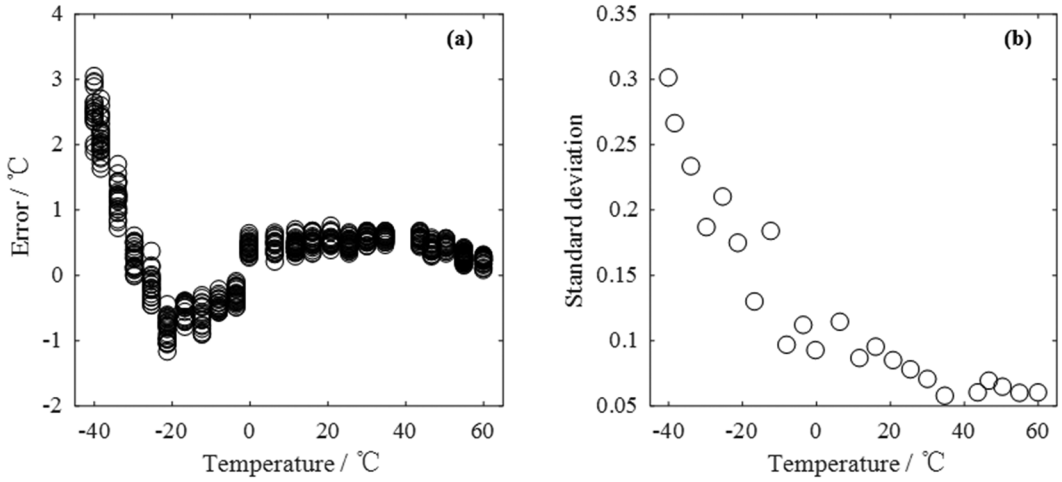

FIG. 4. Measurement results after calibration: (a) errors of different target temperatures and (b) standard deviation of different target temperatures.

c. Uncertainty component introduced by other factors. An estimation of all the other uncertainty components, including environmental factors, leads to $u_{B3} = 0.5\,^{\circ}\mathrm{C}$.

3. Total uncertainty u_C

Combining the standard uncertainty component, the total uncertainty u_C is found,

$$u_c = \sqrt{u_A{}^2 + u_{B1}{}^2 + u_{B2}{}^2 + u_{B3}{}^2} = 1.79\,^{\circ}\mathrm{C}.$$

Taking a covering factor $k = 2$, the expanded uncertainty (at the 95% of confidence level) results in

$$U = 2^{*}u_c = 3.6\,^{\circ}\mathrm{C}.$$

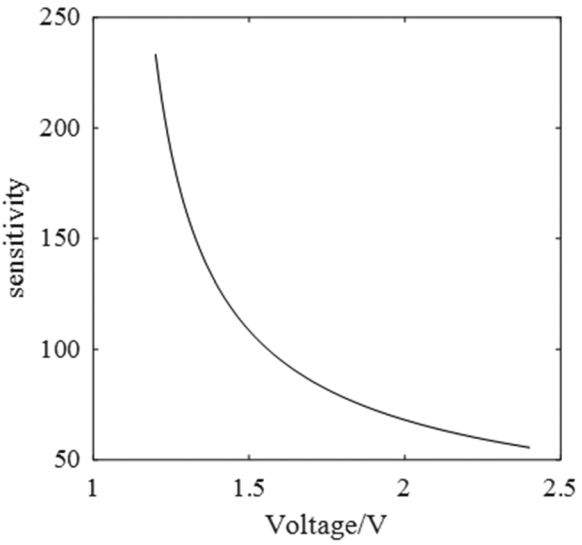

FIG. 5. Sensitivity calculated deriving the calibration function.

D. Compensation function

According to the uncertainty analysis, the contribution of the uncertainty component introduced by calibration accuracy is much larger than other uncertainty components. So, to reduce the uncertainty, it is advisable to start with the uncertainty component introduced by calibration accuracy. Figure 4 shows that the errors of repeated measurements have a typical trend vs the target temperature. This trend presents larger values than the random deviation at the same temperature. Furthermore, it is possible to note that the detector linearity of the data below 0 °C is slightly worse than above 0 °C in Fig. 3. So, it is supposed that a greater deviation between data calculated from the fitting and experimental process could be present due to a nonlinearity of the calibration curve in the low temperature region. During calibration, the calibration fitting process inevitably presents residuals, which can be higher or lower according to the fitting goodness. The factors that affect the linearity of the infrared thermometer output signal include the inherent nonlinearity of the detector, the nonlinearity of the data acquisition circuit, the nonlinearity introduced by the temperature deviation of the blackbody, and the nonlinearity introduced by the emissivity change in the blackbody at different temperatures.[23,24]

Plotting the residuals of the calibration fitting process [Fig. 6(a)] is obtained, and the residuals distributed on both sides of 0 are symmetrical. The sensitivity of the thermometer is calculated deriving the calibration function [Eqs. (1) and (2)] with respect to the temperature, using the Wien approximation and the so-called "effective wavelength," λ_{eff},[22] in the response bandwidth of the detector. It can be expressed by the following equation:

$$\frac{dV}{dT} \approx k c_1 c_2 \frac{\Delta\lambda}{\lambda_{\mathrm{eff}}{}^6 T^2} e^{-c_2/(\lambda_{\mathrm{eff}} T)}. \tag{7}$$

The sensitivity curve of the thermometer is plotted in the range of −40 °C to 60 °C in Fig. 6(b). It shows that the sensitivity decreases rapidly with the decrease in temperature. Thus, the same fitting residuals have different weights at different temperatures (a residual error of 0.01 V at −40 °C leads to a deviation of about 2 °C, and

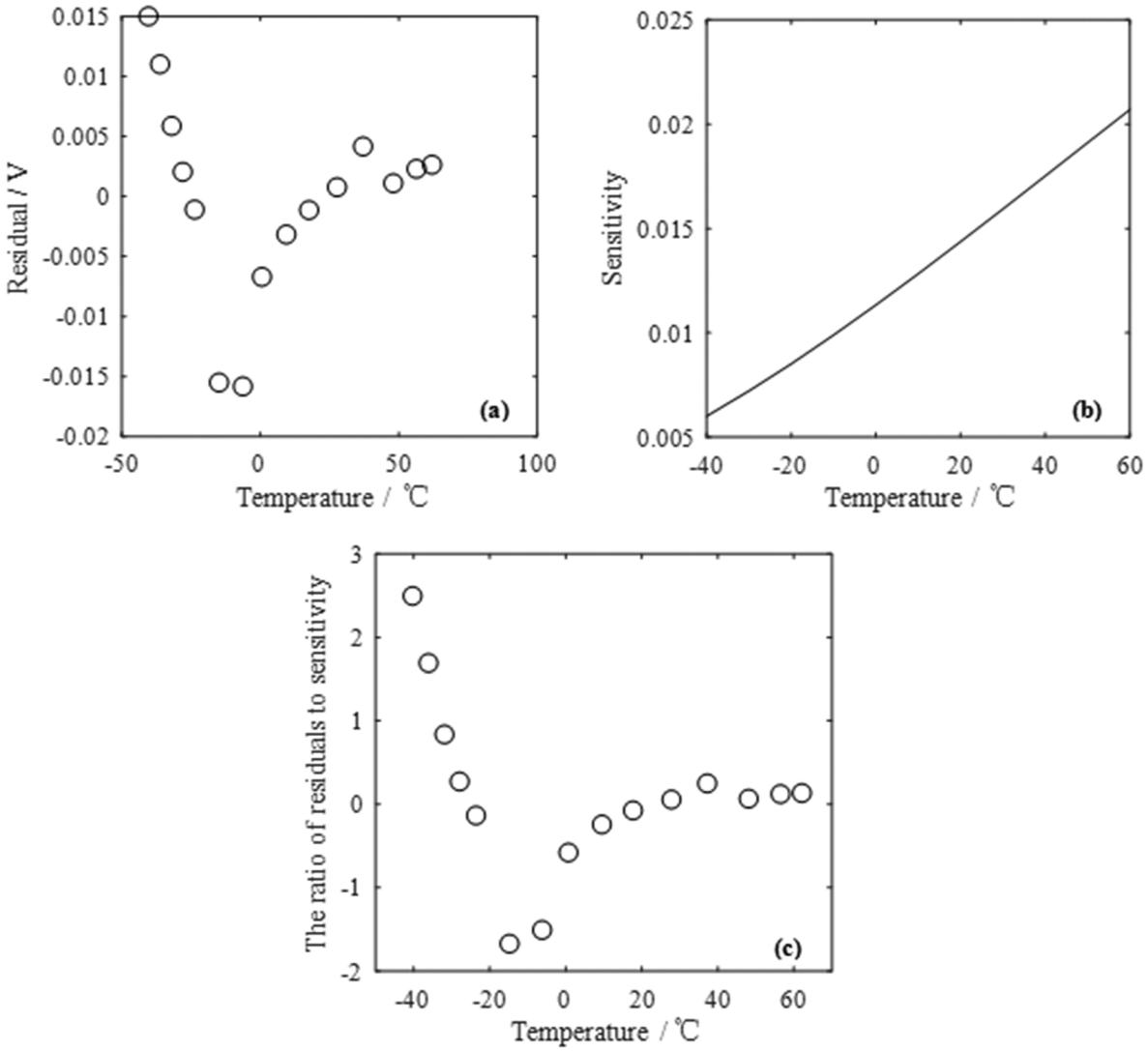

FIG. 6. (a) Calibration fitting residuals, (b) sensitivity of the thermometer, and (c) the ratio of residuals to sensitivity.

the same error at 40 °C leads to a deviation of 0.6 °C). The ratio of residual errors to sensitivity can be used to describe the temperature deviation caused by the residuals, as shown in Fig. 6(c). This trend is consistent with the experimental data of Fig. 4. So, it can be concluded that higher uncertainties are present in the low temperature region and the typical trend of the deviation distribution in Fig. 4 is caused by the residuals weighted by the unfixed sensitivity. (The residuals distributed on both sides of 0 are symmetrical, and the sensitivity is not a constant. The symmetry is broken.)

According to the performed analysis, a meaningful systematic error is present mainly due to a nonlinearity of the calibration curve, evidenced by the fitting residual. In order to improve the measurement accuracy, the fitting residuals could be compensated through a higher order polynomial least squares fit regression, which can take into account the nonlinearity of the recognized residual trend. In the present work, nine-order polynomial was chosen as a fitting model. The results are shown in Fig. 7. This figure shows how the fitting curve basically passes through all the residual points.

Finally, compensation is carried out as follows: First, the voltage collected by using the equipment is compensated. Then, the temperature T of the target is calculated through the infrared temperature measurement [Eqs. (3)–(5)]. After compensation, the accuracy of the temperature measurement is significantly improved. The following equation reports the compensated temperature measurement:

$$T = f^{-1}\left[\frac{\frac{V-\mathrm{delta}(V)-b}{k} - (1-\varepsilon)f(T_u)}{\varepsilon}\right]. \tag{8}$$

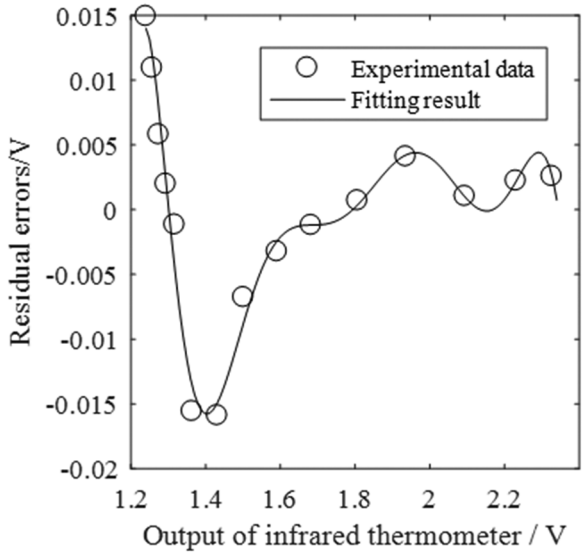

FIG. 7. Fitting result of the compensation function.

Being delta(V), the correction applied comes from Fig. 7.

IV. METHOD VALIDATION

A. Simulation

Data collected in the uncertainty analysis are reprocessed using the compensation function: results are shown in Fig. 8. In Fig. 8, the repeated measurement data still form clouds, but closer to zero than in Fig. 4(a). Deviation after compensation is reduced from ±3.1 °C to ±1.4 °C. This demonstrates the effectiveness of the compensation function.

B. Experiment

Experiments were carried out with the compensation function proposed in this paper. Combining Eqs. (3) and (8), the measurement data after compensation are measured and recorded, as shown in Fig. 9. As shown in Fig. 9, the accuracy is significantly improved after using the compensation function with respect to the measurement data in Fig. 4. Deviation decreases from ±3.1 °C to ±1.5 °C, demonstrating the effectiveness of the compensation function. Measurements were repeated many times at each temperature. The resulting clouds of data presented in Fig. 9 demonstrate that the method is applicable to different temperatures.

The uncertainty analysis shows how the uncertainty changes before and after the application of the compensation function. Clearly, the suggested procedure does not change the type B uncertainties, u_{B2} and u_{B3}. The standard uncertainty of voltage estimation after the application of the compensation function is 0.0037 V. Then, the uncertainty component introduced by calibration accuracy is 0.73 °C, that is, u_{B1} = 0.73 °C. The standard deviation of repeated measurements at each temperature is calculated and shown in Fig. 10. The standard deviation of the repeated measurements depends on temperature and varies between 0.05 °C and 0.37 °C. The maximum value of the standard uncertainty of the mean of the repeated measurements is u_A = std/sqrt(n) = 0.08 °C, where std is the standard deviation and n is the number of repeated measurements.

Combining all the standard uncertainty sources, we get

$$u_c = \sqrt{u_A^2 + u_{B1}^2 + u_{B2}^2 + u_{B3}^2} = 0.94\,^{\circ}\mathrm{C}.$$

Taking k = 2 as the covering factor (95% of confidence level), the expanded uncertainty is

$$U = 2^{*}u_c = 1.9\,^{\circ}\mathrm{C},$$

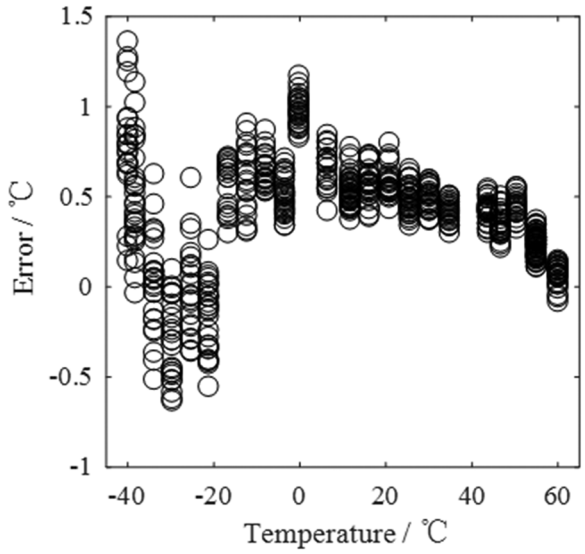

FIG. 8. Compensation simulation: deviation after compensation.

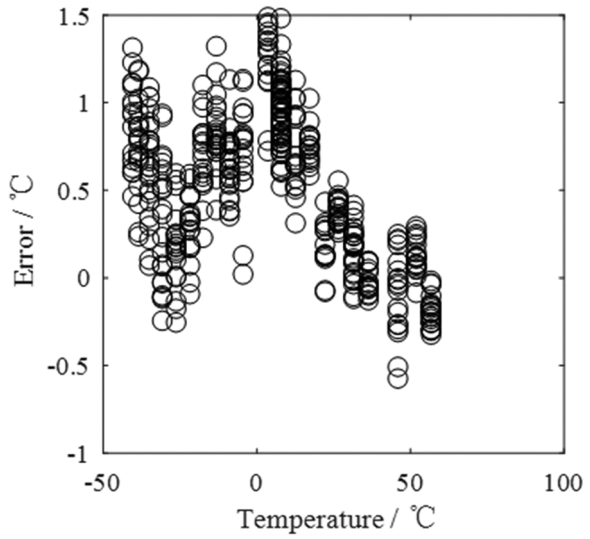

FIG. 9. Experimental data after compensation.

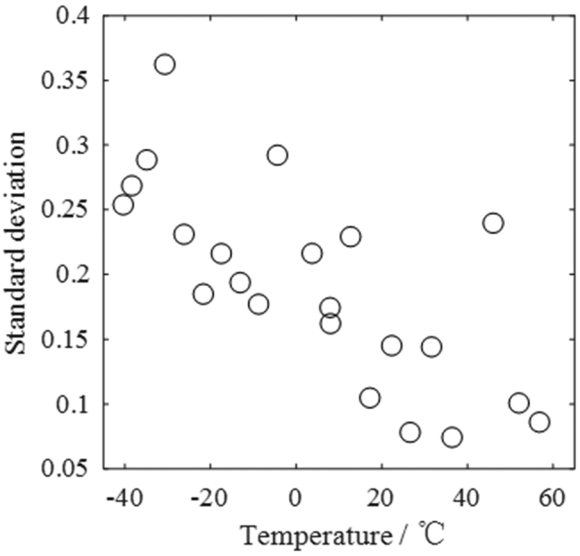

FIG. 10. Standard deviation after compensation.

that is, the compensation function reduces the instrument expanded uncertainty from 3.6 °C to 1.9 °C.

V. CONCLUSION

The present work presents a method for improving the temperature measurement accuracy of an infrared thermometer. The experiments were carried out with a self-developed infrared thermometer and a blackbody. The main uncertainty sources of this infrared thermometer are analyzed, and a compensation function is established to take them into account. The same method to reduce the uncertainty can be applied to other infrared thermometers, after having established the proper compensation function for the tested pyrometer. The experimental results show that the compensation function can reduce the infrared thermometer expanded uncertainty from ±3.6 °C to ±1.9 °C in the temperature range of −40 °C to 60 °C. So, this method can effectively improve the temperature measurement accuracy of the infrared thermometer for the ambient temperature field.

ACKNOWLEDGMENTS

This work was supported by the National Natural Science Foundation of China (Grant No. 61875046).

REFERENCES

[1] Y.-c. Zhang, Y.-m. Chen, and C. Luo, Measurement **74**, 64–69 (2015).
[2] R. W. Helfrich, Proc. SPIE **0178**, 110 (1979).
[3] Y.-W. Zhang, C.-G. Zhang, and V. Klemas, Appl. Opt. **25**, 3683 (1986).
[4] K. Chrzanowski, Infrared Phys. Technol. **36**, 703–713 (1995).
[5] K. Chrzanowski, Infrared Phys. Technol. **37**, 295–306 (1996).
[6] J. Zhang, L. Yang, and H. K. Liu, Infrared Technol. **27**, 419–422 (2005).
[7] Y. C. Zhang, Y. D. Qi, and X. B. Fu, Spectrosc. Spectral Anal. **31**, 3236 (2011).
[8] Y. C. Zhang, Y. D. Qi, and X. B. Fu, Spectrosc. Spectral Anal. **32**, 1241–1246 (2012).
[9] Y. C. Zhang, B. Wei, and X. B. Fu, Spectrosc. Spectral Anal. **34**, 394 (2014).
[10] C. Sun, M. Q. Pan, Y. J. Wang *et al.*, Infrared Technol. **41**, 370–376 (2019).
[11] Q. J. Tian, S. T. Chang, Y. F. Qiao *et al.*, Acta Photonica Sin. **46**, 215–222 (2017).
[12] M. L. Li, X. C. Hu, X. L. Zhen *et al.*, J. Telem., Tracking Command **35**, 61–66 (2014).
[13] ISO/IEC, Guide to the Expression of Uncertainty in Measurement, 2008.
[14] See https://vigo.com.pl/produkty/pvmi-2te/ for VIGO System S.A.; accessed 2017.
[15] T. Svensson, I. Renhorn, and P. Broberg, Proc. SPIE **2009**, 73000Z.
[16] Z. Y. Sun, M. Wang, and S. T. Chang, Laser Infrared **5**, 522–527 (2014).
[17] L. Yang, Infrared Technol. **21**, 20–24 (1999).
[18] P. Coppa, G. Ruffino, and A. Spena, High Temp. - High Pressures **20**, 479–490 (1988).
[19] C. Y. Yang and L. H. Cao, Infrared Laser Eng. **40**, 1624–1628 (2011).
[20] Q. B. Yang, Z. Wei, S. Q. Hu *et al.*, Laser Infrared **48**, 73–78 (2018).
[21] Q. Liu and Z. X. Shao, China Meas. Test **35**, 41–44 (2009).
[22] P. B. Coates, High Temp. - High Pressures **11**, 289–300 (1979).
[23] H. L. Chen, L. C. Hao, R. J. Ding *et al.*, Laser Infrared **42**, 663–666 (2012).
[24] J. X. Mao, Y. L. Ji, H. F. Li *et al.*, Infrared Technol. **41**, 515–520 (2019).